Temperature Measurement in a Bunsen Gas–Droplet Flame of Ethanol Using OH PLIF

D. K. Sharaborin[a,*], **A. S. Lobasov**[a], **R. V. Tolstoguzov**[a], **and V. M. Dulin**[a]

UDC 536.46,543.424.2

Abstract: This paper presents the results of two-line OH planar laser-induced fluorescence (PLIF) thermometry in a laminar conical flame of a gas–droplet mixture of ethanol and air. Laminar flow of a droplet-laden ethanol–air uniform mixture was produced by an ultrasonic atomizer in a vessel filled with liquid ethanol. The properties of the two-phase flow at the nozzle exit without combustion were controlled by a time-shift optical sensor. The temperature field was estimated based on the excitation of the $Q_1(5)$ and $Q_1(14)$ lines of the (1–0) band of the $A^2\Sigma^+$–$X^2\Pi$ electronic system. The spatial nonuniformity of the energy distribution in the laser light sheet illuminating the central plane of the flame cone and the change in the pulse energy from frame to frame were compensated using an additional camera recording the laser light intensity distribution in the calibration cuvette.

Keywords: laminar flame, ethanol combustion, droplet-laden air flow combustion, OH PLIF, planar thermometry, two-line OH PLIF.

INTRODUCTION

Currently, stringent requirements are placed on the efficiency, environmental friendliness, and level of air pollution from power plants and units based on gaseous and liquid fuel combustion. The development of new systems and updating of existing ones is impossible without a clear representation of the physical processes occurring in combustion chambers. Full-scale experiments in real conditions are most often unreasonably expensive and technically difficult to conduct. For this reason, methods of numerical simulation are used to develop new burners and combustion chambers. However, the results of numerical simulation methods, in particular combustion simulation methods, need to be verified by simple physical realizations.

Combustion in droplet-laden two-phase flows is more difficult to numerically simulate and mathematically describe than the combustion of gas mixtures since it involves not only chemical reactions and gas phase transfer, but also transport processes during the motion and interaction of liquid droplets, their heating, and evaporation. The effect of these processes on combustion has been considered in a number of review papers (see [1–4]). As a rule, the ignition [5–8] and propagation of the flame front [9–12] have been studied in basic experimental configurations with steady-state constant flow of a fully mixed mixture with uniformly distributed liquid fuel droplets. The most common basic configurations are a laminar conical flame [13], a counterflow diffusion flame [2, 14, 15], and a strained flame stabilized by flow impingement on a solid surface [16, 17].

In this paper, the emphasis is on planar temperature measurements using laser-induced fluorescence (PLIF) in a conical laminar flame of a gas–droplet mixture of ethanol vapor with air. The PLIF method

---

[a]Kutateladze Institute of Thermophysics, Siberian Branch, Russian Academy of Sciences, Novosibirsk, 630090 Russia;
*Sharaborin.d@gmail.com.
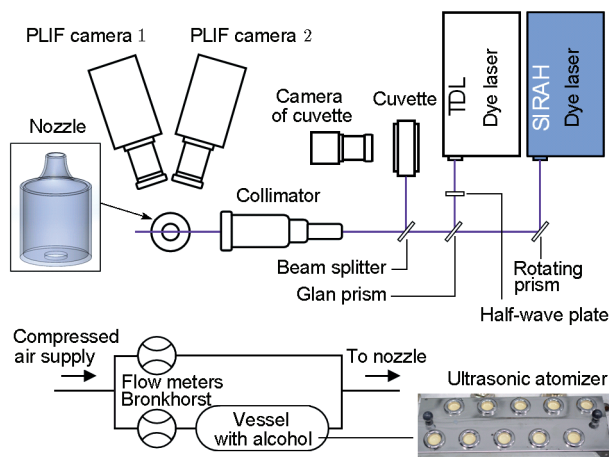
Fig. 1. Diagram of the experimental setup and the system for preparation of the gas–droplet mixture.

based on the excitation of two different transitions of the hydroxyl radical (two-line OH PLIF) has become a common method for estimating temperature in combustion products [18–21]. Different papers report on the use of different transitions to excite fluorescence signals [22–25]. The most widely used are the pairs of transitions $P_1(2) : R_2(13)$ and $Q_1(5) : Q_1(14)$ [18, 21, 24, 25]. As noted previously [26], the pair $Q_1(5) : Q_1(14)$ of those considered in the paper has the highest ratio of the recorded signals and provides a good agreement in temperature with the values measured by the spontaneous Raman scattering method, which makes this pair most suitable for temperature measurements based on the excitation of the (1–0) band of the $A^2\Sigma^+–X^2\Pi$ system.

The purpose of this work is to obtain new experimental data for a conical laminar flame (Re = 1000) of a droplet-laden ethanol–air mixture at different equivalence ratios (ϕ = 0.95 and 1.2). The data obtained can be further used to verify numerical models. In addition, the planar temperature measurement method based on recording the OH PLIF signal in the gas–droplet flame was validated and tested. The spatial convergence and calibration of the radiation sources and recording systems of the two combined PLIF systems are described. The characteristics of the two-phase nonreacting flow were measured using the time-shift method [27].

1. EXPERIMENTAL

1.1. Experimental Setup and Measuring Equipment

The measurements were carried out in a laminar conical premixed flame stabilized at the exit of an axisymmetric converging nozzle. The three-dimensional

nozzle geometry (without a swirler) is described in detail in [28], and the three-dimensional model is shown in Fig. 1. The Reynolds number of the flow issuing from a nozzle with a diameter of 15 mm was Re = 1000 (calculated for a flow rate of 10.8 liters/min and the viscosity of air at room temperature). A mixture of vapors and a dispersion of ethanol droplets mixed with dry air was used as a fuel. The choice of ethanol as a fuel is due to the relative safety of its storage and use compared to other liquid fuels. In addition, ethanol combustion is described by a smaller number of intermediate chemical reactions than other liquid fuels (e.g., kerosene), which simplifies the use of ethanol as a model fuel in numerical simulation. Fuel was supplied by passing air through a vessel with ethanol. At the bottom of the vessel was an ultrasonic atomizer (KERI M1009-2) consisting of ten piezoelectric membranes assembled in a single housing with an electronic unit generating a 1.7 MHz frequency signal. Similar units are used in industrial humidifiers. At a maximum air flow rate through the vessel, complete replacement of gas in the vessel (approximately 50 liters, ten of which are liquid ethanol) takes quite a long time ($\approx$4 min). The manufacturer's claimed performance (volume of water converted in total to vapor and aerosol) of the ultrasonic atomizer is 9 liters/h, which far exceeds the amount of ethanol vapor carried away from the vessel by air (1.6 g/min of ethanol vapor at an air flow rate of 10.8 liters/min). This made it possible to provide the equilibrium concentration of saturated ethanol vapor in air in the vessel volume. The main flow of air with ethanol vapor and droplets could be diluted with an additional flow of dry air to change the equivalence ratio at the nozzle outlet. To ensure better mixing of the main and additional airflows, the nozzle was connected to the system through a long (70 cm) mixer tube. The air flow was controlled with mass flow meters (Bronkhorst El-Flow). The size and velocity of ethanol droplets at the nozzle outlet was measured using a time-shift optical ranging system (AOM Systems SpraySpy). The average droplet size was 14 μm.

Flame temperature was estimated by the two-line OH PLIF technique (see Fig. 1) using two independent OH PLIF systems synchronized by a pulse generator (BNC 575 model). One of the PLIF systems consisted of a tunable dye laser (Sirah Precision scan), a Nd:YAG pulsed pump laser (QuantaRay, an energy of approximately 0.7 J per pulse at a wavelength of 532 nm) and an UV sensitive intensified CCD camera (PCO Dicam Pro, 12-bit images with a resolution of 1280 × 1024 pixel). The other system also consisted of a tunable dye laser (Quantel TDL+), a Nd:YAG pump laser (Quantel YG980 with an energy of 0.5 J per pulse at a wavelength of 532 nm), and a camera (LaVi-

sion imager sCMOS, 16-bit images with a resolution of 2560×2160 pixel) connected to an amplifier (LaVision IRO). The intensified cameras were equipped with UV lenses (LaVision 100 mm, f# = 2.8) and bandpass optical filters (LOT-Oriel with a transmittance of 17% at a wavelength of 310 nm with a FWHM of 11 nm).

The two-line OH PLIF technique was implemented using a combination of the $Q_1(5)$ and $Q_1(14)$ lines of the (1–0) band of the $A^2\Sigma^+–X^2\Pi$ electronic system, which, according to [26], is one of the most effective pairs. The average energy of tunable laser pulses for these transitions was approximately 3 and 15 mJ, respectively. To ensure that the laser wavelengths corresponded to the excitation wavelengths, the OH radical excitation spectrum was scanned and calibrated by comparison with the simulation results using LifBase software [29]. The laser beams of the two PLIF systems were reduced to a single optical path using a Glan–Taylor (Thorlabs) prism and a half-wavelength plate, after which the beams were deployed into a collimated laser light sheet 50 mm wide and 0.8 mm thick in the measurement area. The optimal spatial coincidence of the laser light sheets was controlled using photo paper before the experiment. Two laser pulses of the PLIF systems were separated in time by 0.6 μs. The exposure time of both PLIF cameras was 200 ns. An additional CCD camera (ImperX Bobcat IGV-B4820, 12-bit images) controlled the fluorescence intensity inside the rectangular cuvette filled with a Rhodamine 6G solution to take into account the nonuniformity of the energy distribution in both laser light sheets. Part of the laser radiation was reflected ($\approx$4%) into the cuvette with a translucent mirror placed after the collimator. The spatial convergence of images from the PLIF cameras to a single coordinate system was carried out using a plane calibration target (Edmund optics). The target was a 100×100 mm white scattering plate with black round markers of 1 mm diameter located on a regular grid with a node spacing of 2 mm. Image projection transforms for each camera were approximated by third-order polynomials [30].

1.2. Processing of Experimental Data

After correction of perspective distortions, the PLIF images were processed by a set of mathematical algorithms, including a correction of the spatial nonuniformity in the laser light sheet energy distribution and in the sensitivity of the recording arrays of the cameras. In addition, the images were processed to remove the background, shadow current, and reflections (examples are shown in Figs. 2–5). The nonuniform sensitivity of detectors was taken into account by recording white paper placed out of focus and evenly lit. The background

was evaluated by recording PLIF images when the laser illuminated the measurement plane without flame and droplets. The spatial resolution of the PLIF systems was 31.42 and 15.11 pixels/mm. To control the spatial distribution of the laser light sheet intensity, which is necessary for correcting the PLIF data, we used a rectangular quartz cell with a Rhodamine 6G solution in water.

3. RESULTS

For two-line PLIF thermometry, OH fluorescence was excited on two different lines of transitions from the $X^2\Pi$ ground state. The intensity ratio of the fluorescence signals (S_1 and S_2) is related to the temperature T assuming a Boltzmann distribution of the population of the ground states [24]:

$$\frac{S_1}{S_2} = \frac{B_1 I_1 (2J_1+1)}{B_2 I_2 (2J_2+1)} \exp\left(-\frac{E_1 - E_2}{kT}\right). \qquad (1)$$

Here J_1 and J_2 are the rotational quantum numbers of the excited transitions 1 and 2 for the ground states with energies E_1 and E_2, respectively, B_1 and B_2 are the Einstein absorption coefficients, and I_1 and I_2 are local values of the laser radiation energy density estimated based on images in the cuvette.

Figure 6 shows photographs of the laminar conical flame (Re = 1000) with equivalence ratios $\phi = 0.95$ and 1.2. Figure 7 shows three examples of the ratio of instantaneous distributions of PLIF signals for two lines $(S_1 I_2)/(S_2 I_1)$ for $\phi = 0.95$ at different times. Figure 8 shows an estimate of the instantaneous temperature distribution for the same case. Similar examples for $\phi = 1.2$ are given in Figs. 9 and 10. The data show that the mixing layer between ambient air and the hot mixture of combustion products above the flame front is distorted and oscilated due to the natural convection resulting from the action of buoyancy forces. The flame temperature varies in the range 1200–2100 K, with the lowest values observed in the outer layer of mixing with ambient air. It should be noted that data analysis and temperature estimation are possible only in the region containing hot OH radicals, so the regions without signals are highlighted in white in the images.

Figure 11 shows the time-averaged temperature distributions obtained from 500 instantaneous temperature realizations for each case. The distributions show no significant influence of laser radiation absorption along the axis of laser light sheet propagation. It is found that the root-mean-square temperature fluctuations behind the flame front are in the range 100–150 K. They are mainly caused by the noise of the recording system, which can be reduced by image binning at the
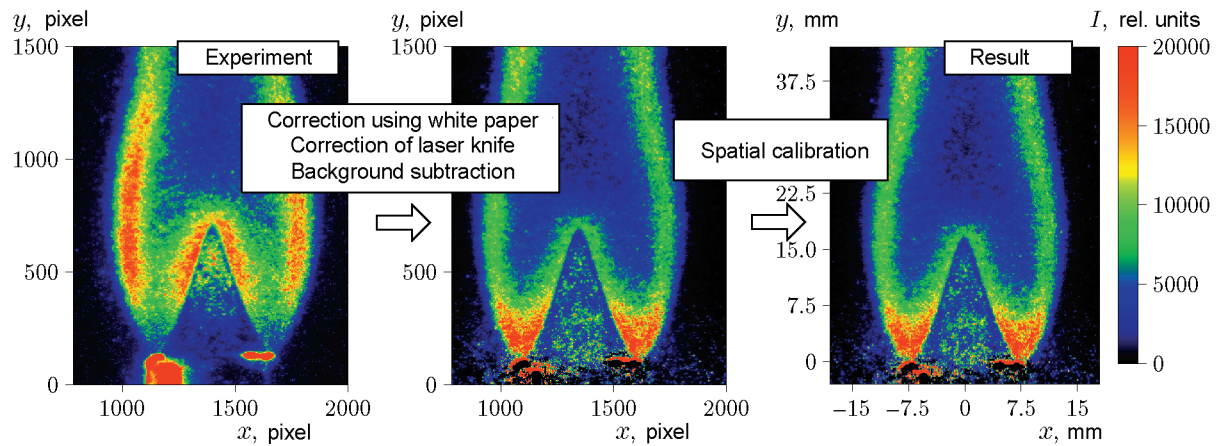
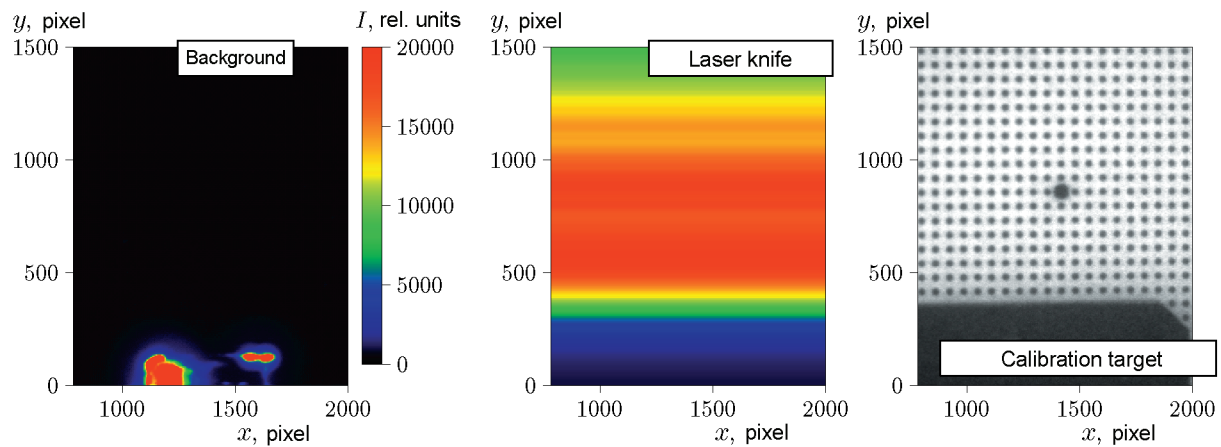**Fig. 2.** Example of processing for the excitation of the $Q_1(14)$ line.

Fig. 3. Examples of the background image and intensity distributions in the laser light sheet and calibration target in the case of excitation of the $Q_1(14)$ line.
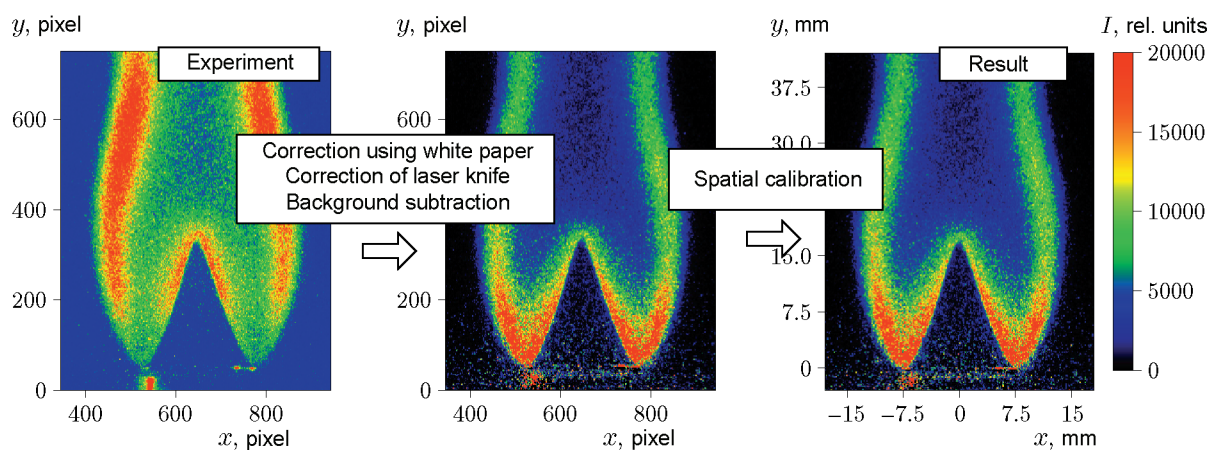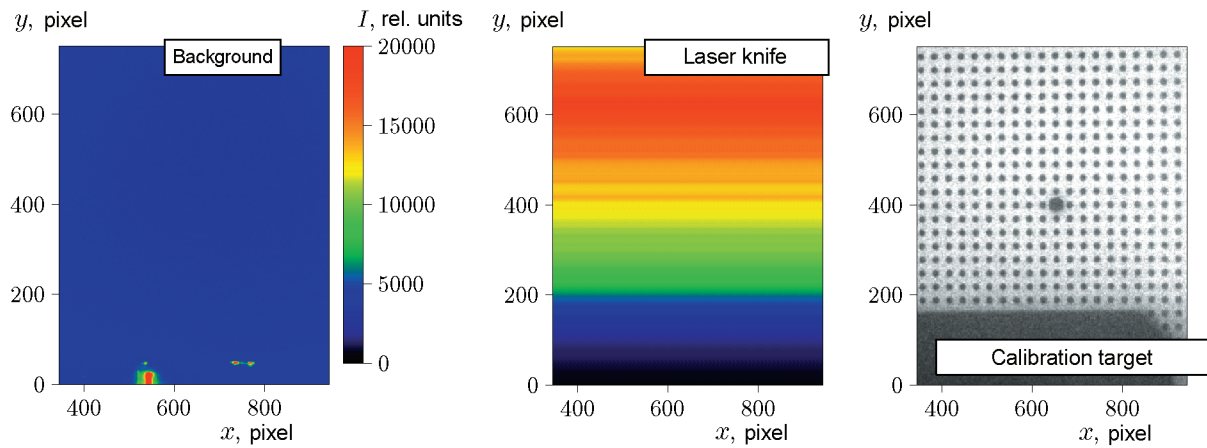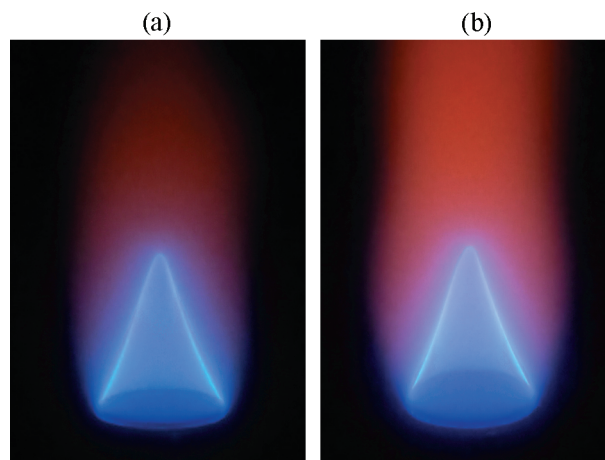

Fig. 4. Example of processing for the excitation of the $Q_1(5)$ line.

Fig. 5. Examples of the background image and intensity distributions in the laser light sheet and calibration target in the case of excitation of the $Q_1(5)$ line.

Fig. 6. Photographs of the investigated laminar flame (Re = 1000) for $\phi = 0.95$ (a) and 1.2 (b).
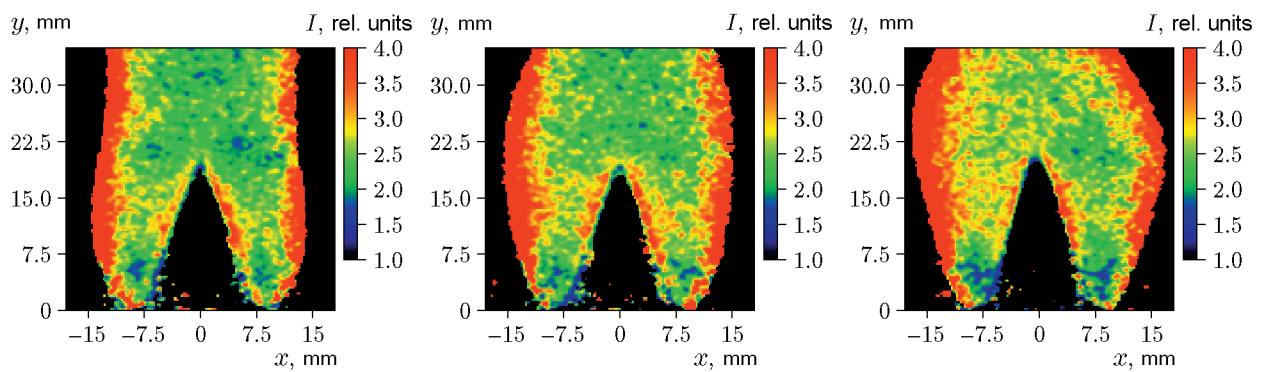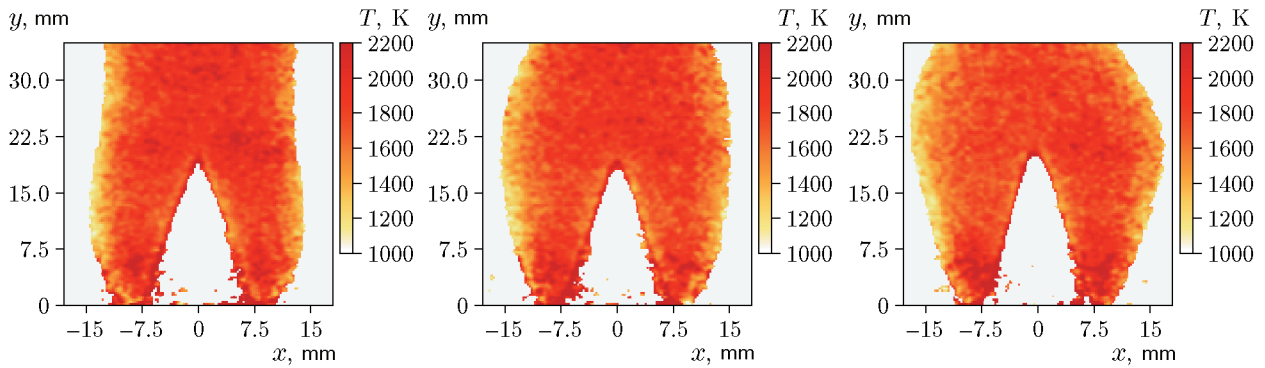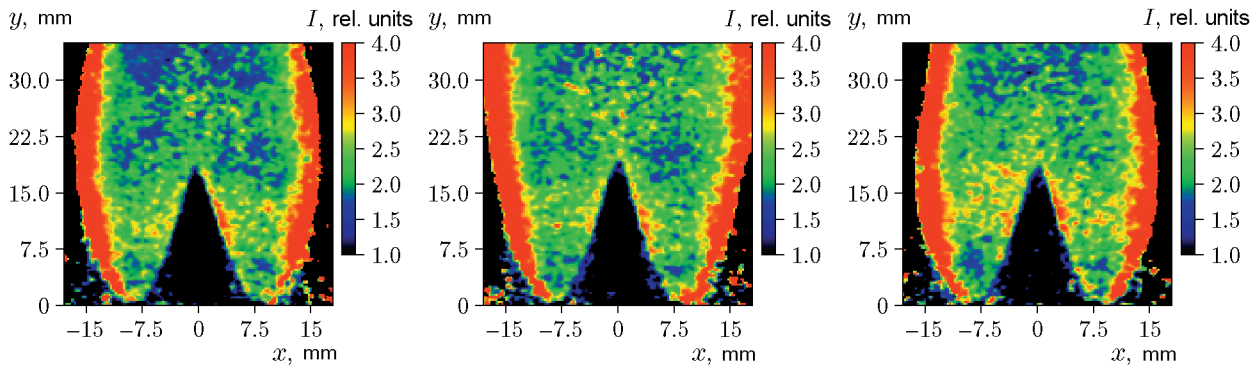

Fig. 7. Examples of the ratio of instantaneous PLIF signals of the $Q_1(5)$ and $Q_1(14)$ lines recorded at different times for Re = 1000 and $\phi = 0.95$.
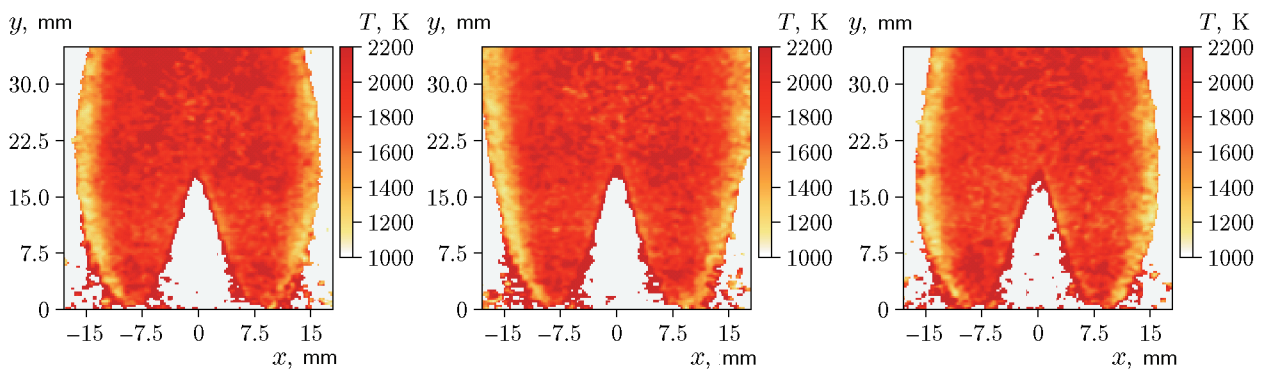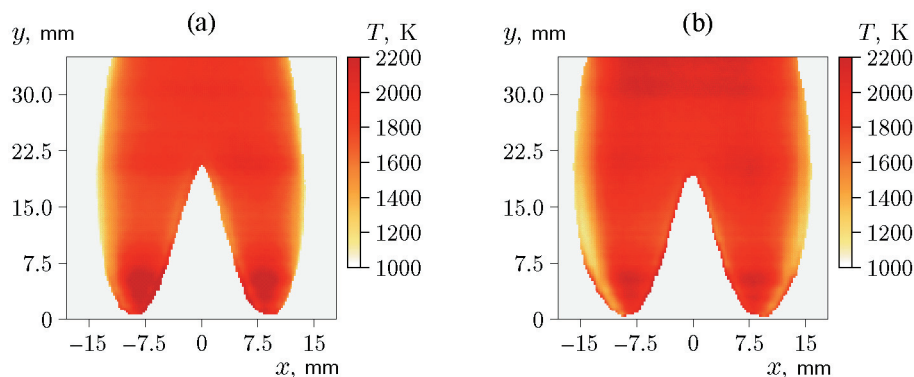
Fig. 8. Examples of instantaneous temperature distributions recorded at different times for Re = 1000 and $\phi = 0.95$.
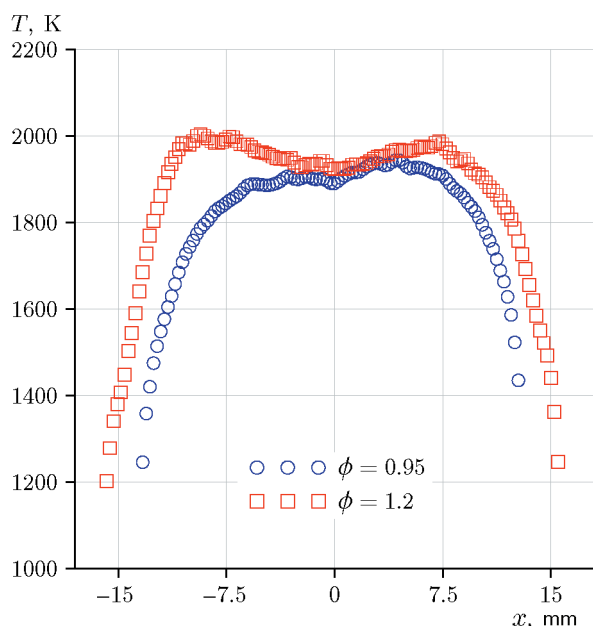

Fig. 9. Examples of the ratio of instantaneous PLIF signals of the $Q_1(5)$ and $Q_1(14)$ lines recorded at different times for Re = 1000 and $\phi = 1.2$.

Fig. 10. Examples of instantaneous temperature distributions recorded at different times for Re = 1000 and $\phi = 1.2$.

Fig. 11. Average temperature distributions under the investigated conditions Re = 1000 and $\phi = 0.95$ (a) and 1.2 (b).

Fig. 12. Average temperature profiles in the section at a height of 25 mm above the nozzle exit.

hardware level. Figure 12 shows the cross section of the temperature distribution in the flame at a height of 25 mm above the nozzle exit. As expected, the flame temperature profile in the fuel-rich combustion mode is wider due to the additional reaction zone near the outer mixing layer, where excess fuel not burned in the flame front is oxidized.

CONCLUSIONS

Temperature in a droplet-laden ethanol–air laminar conical flame was estimated using two-line OH PLIF. Realizations of the temperature field were estimated by mathematical processing with a time resolution of approximately 0.6 μs. The root-mean-square temperature fluctuations behind the laminar conical flame front due to the noise of the recording system were up to 150 K and could be reduced without a significant loss of spatial resolution by image binning at the hardware level.

REFERENCES

1. W. A. Sirignano, "Fuel Droplet Vaporization and Spray Combustion Theory," Prog. Energy Combust. Sci. **9** (4), 291–322 (1983); DOI: 10.1016/0360-1285(83)90011-4.

2. S. C. Li, "Spray Stagnation Flames," Prog. Energy Combust. Sci. **23** (4), 303–347 (1997); DOI: 10.1016/S0360-1285(96)00013-5.

3. P. Jenny, D. Roekaerts, and N. N. Beishuize, "Modeling of Turbulent Dilute Spray Combustion," Prog. Energy Combust. Sci. **38** (6), 846–887 (2012); DOI: 10.1016/j.pecs.2012.07.001.

4. A. R. Masri, "Turbulent Combustion of Sprays: from Dilute to Dense," Combust. Sci. Technol. **188** (10), 1619–1639 (2016); DOI: 10.1080/00102202.2016.1198788.

5. D. R. Ballal and A. H. Lefebvre, "Ignition and Flame Quenching of Flowing Heterogeneous Fuel–Air Mixtures," Combust. Flame **35**, 155–168 (1979); DOI: 10.1016/0010-2180(79)90019-1.

6. A. M. Danis, I. Namer, and N. P Cernansky, "Droplet Size and Equivalence Ratio Effects on Spark Ignition of Monodisperse *n*-Heptane and Methanol Sprays," Combust. Flame **74** (3), 285–294 (1988); DOI: 10.1016/0010-2180(88)90074-0.

7. P. M. De Oliveira, P. M. Allison, and E. Mastorakos, "Ignition of Uniform Droplet-Laden Weakly Turbulent Flows Following a Laser Spark," Combust. Flame **199**, 387–400 (2019); DOI: 10.1016/j.Combustflame.2018.10.009.

8. P. M. De Oliveira and E. Mastorakos, "Mechanisms of Flame Propagation in Jet Fuel Sprays As Revealed by OH/Fuel Planar Laser-Induced Fluorescence and OH* Chemiluminescence," Combust. Flame **206**, 308–321 (2019); DOI: 10.1016/j.combustflame.2019.05.005.

9. S. Hayashi, S. Kumagai, and T. Sakai, "Propagation Velocity and Structure of Flames in Droplet–Vapor–Air Mixtures," Combust. Sci. Technol. **15** (5/6), 169–177 (1977); DOI: 10.1080/00102207708946782.

10. G. A. Richards and A. H. Lefebvre, "Turbulent Flame Speeds of Hydrocarbon Fuel Droplets in Air," Combust. Flame **78** (3/4), 299–307 (1989); DOI: 10.1016/0010-2180(89)90019-9.

11. H. Nomura, I. Kawasumi, Y. Ujiie, and J. I. Sato, "Effects of Pressure on Flame Propagation in a Premixture Containing Fine Fuel Droplets," Proc. Combust. Inst. **31** (2), 2133–2140 (2007); DOI: 10.1016/j.proci.2006.07.036.

12. D. Bradley, M. Lawes, S. Liao, and A. Saat, "Laminar Mass Burning and Entrainment Velocities and Flame Instabilities of *i*-Octane, Ethanol and Hydrous Ethanol/Air Aerosols," Combust. Flame **161** (6), 1620–1632 (2014); DOI: 10.1016/j.Combustflame.2013.12.011.

13. J. H. Burgoyne and L. Cohen, "The Effect of Drop Size on Flame Propagation in Liquid Aerosols," Proc. R. Soc. A **225** (1162), 375–392 (1954); DOI: 10.1098/rspa.1954.0210.

14. G. Chen and A. Gomez, "Counterflow Diffusion Flames of Quasi-Monodisperse Electrostatic Sprays," Proc. Combust. Inst. **24** (1), 1531–1539 (1992); DOI: 10.1016/S0082-0784(06)80178-5.

15. N. Darabiha, F. Lacas, J.C. Rolon, and S. Candel, "Laminar Counterflow Spray Diffusion Flames: A Comparison between Experimental Results and Complex Chemistry Calculations," Combust. Flame **95** (3), 261–275 (1993); DOI: 10.1016/0010-2180(93)90131-L.

16. C. T. Chong and S. Hochgreb, "Measurements of Laminar Flame Speeds of Acetone/Methane/Air Mixtures," Combust. Flame **158** (3), 490–500 (2011); DOI: 10.1016/j.Combustflame.2010.09.019.

17. L. Fan, B. Tian, C. T. Chong, et al., "The Effect of Fine Droplets on Laminar Propagation Speed of a Strained Acetone–Methane Flame: Experiment and Simulations," Combust. Flame **229**, 111377 (2021); DOI: 10.1016/j.Combustflame.2021.02.023.

18. R. Giezendanner-Thoben, U. Meier, W. Meier, and M. Aigner, "Phase-Locked Temperature Measurements by Two-Line OH PLIF Thermometry of a Self-Excited Combustion Instability in a Gas Turbine Model Combustor," Flow Turbul. Combust. **75** (1–4) 317–333 (2005); DOI: 10.1007/s10494-005-8587-0.

19. B. Ayoola, G. Hartung, C. A. Armitage, et al., "Temperature Response of Turbulent Premixed Flames to Inlet Velocity Oscillations," Exp. Fluids **46** (1) 27–41 (2009); DOI: 10.1007/s00348-008-0534-0.

20. Z. Yang, X. Yu, J. Peng, et al., "Effects of N_2, CO_2 and H_2O Dilutions on Temperature and Concentration Fields of OH in Methane Bunsen Flames by Using PLIF Thermometry and Bi-Directional PLIF," Exp. Therm. Fluid Sci. **81**, 209–222 (2017); DOI: 10.1016/j.Expthermflusci.2016.10.017.

21. B. R. Halls, P. S. Hsu, S. Roy, T. R. Meyer, and J. R. Gord, "Two-Color Volumetric Laser-Induced Fluorescence for 3D OH and Temperature Fields in Turbulent Reacting Flows," Opt. Lett. **43** (12), 2961–2964 (2018); DOI: 10.1364/OL.43.002961.

22. J. M. Seitzman, R. K. Hanson, P. A. DeBarber, and C. F. Hess, "Application of Quantitative Two-Line OH Planar Laser-Induced Fluorescence for Temporally Resolved Planar Thermometry in Reacting Flows," Appl. Opt. **33** (18), 4000–4012 (1994); DOI: 10.1364/AO.33.004000.

23. E. J. Welle, W. L. Roberts, C. D. Carter, and J. M. Donbar, "The Response of a Propane–Air Counter-Flow Diffusion Flame Subjected to a Transient Flow Field," Combust. Flame **135** (3), 285–297 (2003); DOI: 10.1016/S0010-2180(03)00167-6.

24. R. Devillers, G. Bruneaux, and C. Schulz, "Development of a Two-Line OH-Laser-Induced Fluorescence Thermometry Diagnostics Strategy for Gas-Phase Temperature Measurements in Engines," Appl. Opt. **47** (31) 5871–5885 (2008); DOI: 10.1364/AO.47.005871.

25. S. Kostka et al., "Comparison of Line-Peak and Line-Scanning Excitation in Two-Color Laser-Induced-Fluorescence Thermometry of OH," Appl. Opt. **48** (32), 6332–6343 (2009); DOI: 10.1364/AO.48.006332.

26. A. S. Lobasov, R. V. Tolstoguzov, D. K. Sharaborin, L. M. Chikishev, and V. M. Dulin, "On the Efficiency of Using Different Excitation Lines of (1–0) Two-Line OH Fluorescence for Planar Thermometry," Teplofiz. Aeromekh. **28** (5), 793–797 (2021) [Thermophys. Aeromech. **28** (5), 751–755 (2021); https://doi.org/10.1134/S0869864321050176].

27. W. Schäfer and C. Tropea, "Time-Shift Technique for Simultaneous Measurement of Size, Velocity, and Relative Refractive Index of Transparent Droplets or Particles in a Flow," Appl. Opt. **53** (4), 588–597 (2014); DOI: 10.1364/AO.53.000588.

28. A. S. Lobasov, S. V. Alekseenko, D. M. Markovich, and V. M. Dulin, "Mass and Momentum Transport in the near Field of Swirling Turbulent Jets. Effect of Swirl Rate," Int. J. Heat Fluid Flow **83**, 108539 (V); DOI: 10.1016/j.ijheatfluidflow.2020.108539.

29. J. Luque and D. Crosley, "Lifbase: Database and Spectral Simulation (Version 1.5)," SRI Int. Report No. MP 99-009 (1999).

30. S. M. Soloff, R. J. Adrian, and Z. C. Liu, "Distortion Compensation for Generalized Stereoscopic Particle Image Velocimetry," Meas. Sci. Technol. **8** (12), 1441–1454 (1997).